Atomistic Simulations of Interfacial deformation and bonding mechanism of Pd-Cu Composite Metal Membrane using Cold Gas Dynamic Spray Process.

Sunday Temitope Oyinbo[1], Tien-Chien Jen*[1], Yudan Zhu[2], Joseph Sehinde Ajiboye[3], Sikiru Oluwarotimi Ismail[4]

[1]Department of Mechanical Engineering Science, University of Johannesburg, South Africa.

[2]College of Chemical Engineering, Nanjing Tech University, Nanjing, China

[3]Department of Mechanical Engineering, University of Lagos, Nigeria

[4]School of Engineering and Computer Science, University of Hertfordshire, United Kingdom

*corresponding author.

Jen, Tien-Chien

Department of Mechanical Engineering Science, University of Johannesburg, Gauteng, 2006, South Africa

E-mail address: tjen@uj.ac.za

Abstract

The creation of atomic structures and the study of the deformation processes through molecular dynamics simulations have shown many advantages. However, gaps associated with the development and evolution of microstructure in the coating zone and dynamic processes that take place during cold gas dynamic sprayed materials still exist. The focus of this study was to investigate the interfacial deformation behaviours and the mechanism of bonding between atoms of palladium (Pd) and copper (Cu) composite metal membrane (CMM) using molecular dynamic

simulations. The results confirmed that asymmetric deformation occurred during cold gas dynamic spray at the Pd-Cu interfacial region. As the impact time increases, the layer thickness at the interface also increases. The concentrations of Pd-Cu CMM at the interfacial zone showed the presence of phase transitions at relatively long impact time. Furthermore, CGDS deformation was found to be an unsteady and dynamic process. Explicit bond analysis in this study also has shown that breaking of atomic bonds is not the key mechanism for the initial Pd-Cu plastic deformation occurrence. The higher interfacial bonding energy and interfacial shearing strength at the Pd-Cu CMM interface expressed the bonding strength and compatibility of Pd and Cu.

Keywords: Molecular dynamics; CGDS; shear plastic-deformation: Bond mechanism

1.0 Introduction

The mechanism of cold gas dynamic spray (CGDS) is due to the technique of solid-state deposition. This feature makes CGDS perfect for various applications in engineering involving composites, ceramic, polymers and metals. The incremental plastic deformation produces by the effect of impact velocity of the accelerating powder through the converging-diverging nozzle is achieved by the pressure gas expansion through the nozzle. Thereby, creating metallurgical coalescence between the substrate and the particle [1–4]. Particles plastically deform and form a uniform layer when they impact the target surface (substrate). The particle/substrate bonding will occur only when the speed of the sprayed particles approaches a level called critical velocity under some operating conditions [2,5]. Nanoscale cold gas dynamic spraying is a possible technology to deposit or coat nanostructured materials on a substrate surface without any noticeable effect on their properties or structure [5–8]. The technology has major applications in the critical fields of engineering including composite metal matrix (CMM), plastic, ceramic and metallic coatings [5,7,9,10]. The bonding of materials during the process of cold gas dynamic spray deposition occurs at the atomic level [11–13]. The material's suitability for CGDS depends on their mechanical and physical properties, including the strength of the material, density, melting hardness and melting temperature [6,7,14–16]. Materials such as copper aluminium with relatively low yield capacity are considered desirable for CGDS because they exhibit relatively greater softening at elevated temperatures [6,14], whereas the CGDS has not been ideal with high resistance materials because of the lack of enough deformation capacity.

Research at the atomistic level has drawn increasing attention with the rapid advances in computer technology and the molecular dynamics (MD) [17–20]. The MD method clearly shows

several benefits to demonstrate the evolution of atomic structures and analysis at the microscopic level of deformation mechanisms. It has therefore been used during coating processes to study phenomena related to plastic deformation. The fact that the complex mechanisms in the CGDS process take place at the atomistic level within a relatively short time (nanoseconds) can be explained using MD. In such cases, simulation techniques such as approaches with numerical methods and finite element analysis (FEA) were also used as an alternative. During the CGDS process and thermal spray techniques, FEA was widely employed to understand the influence of process parameters at the macroscale level [21–23]. The CGDS process was investigated using ABAQUS/Explicit program, to study the impact dynamics, critical velocities and bonding mechanism [24]. The study concluded that the critical velocity of sprayed material depends on the preheating temperature, type of sprayed particle, particle size, particle quality and friction coefficient [24]. Thermal process splat formation was studied using a numerical modelling technique which confirmed that changes in the temperature of the substrate minimize splat formation [25]. ABAQUS/Explicit, an FEA tool used for CGDS simulation, has shown that the production of the shear localization requires minimal initial particle velocity [3,26,27]. It is widely recognized that when solid powder deforms and plastically deform on the substrate during CGDS, the actual bonding mechanism is still unclear [26]. According to Assadi *et al*. [28], particles adhere solely to the substrate after impact due to their kinetic energy. Their analysis showed that bonding can be attributed to adiabatic shear instability occurring on or above the critical velocity of the particle surface. Xie *et al.* [29] suggested a new theory that would explain the coating mechanism and interfacial bonding between hard Ni and soft Al substrates experimentally. They found that metal to metal deformation and interfacial bonding results from the breaking of cracked oxides reimaging at the interfacial zone of particle/substrate

by particle peening effects into nano-piece. Hassani-Gangaraj *et al*. [30], argued that the well-built interfacial strain required for bonding does not essentially need adiabatic shear instability. They rather propose that the connection of strong pressurizing waves with the unrestricted interface on the particle edges, a rapid-impact dynamic effect, can produce hydrodynamic plasticity that binds, without requiring shear instabilities.

Finite element studies cannot adequately describe the deformation mechanism [31]. During the CGDS process, Molecular Dynamics (MD) simulation is considered to be an exceptional tool in studying the molecular bonding and deformation processes which occurs at the atomic level [32]. The atomic or molecular interaction during MD simulation is evaluated by the classical movement equations. Nonetheless, few studies were reported in the literature using molecular simulations to investigate the actual mechanisms of deformation and bonding in the CGDS deposition process. One of these research studies used molecular dynamics simulation to evaluate the effect of particle impact velocity during CGDS on Titanium/Nickel, particles/substrate coating processes [33]. The analysis showed a stronger bond at the interface of the particle and the substrate due to increased impact speeds. MD simulation has also been used for the study of the structural-property relationship for thermal spray processes [34]. The studies showed that as the flow fluid Reynolds number increases, the splat diameter and maximum height increased until a critical value after impact was reached. Aneesh and Sagil [32] studied the interaction between metal/metal using Cu material to investigate various process parameters, for example, impact angles, particle size as well as initial impact speed, at the atomic level. Their findings have shown that the highest deposition efficiency and quality were achieved at the initial impact velocity between 500 m/s and 700 m/s, 90° impact angle and particle size of 0.2 nm. The stability and structure of Pd particles were studied by Rojas *et al.* [35] on the Pt [h k l]

and Au [h k l] surfaces at different degrees and discovered that along with the crystallographic orientation of the substrate, the Pd adlayers grew pseudo morphically and epitaxially. Another investigation was carried out by Guo *et al*.[36] on the Pd islands growth on the surface of Nickel substrate with orientation [1 1 1] direction. They found out that with 0.4 monolayers or less of the Pd coverage, 2-dimensional mechanism of the growth appeared while 3-dimensional islands occur at the higher monolayer. The behaviours of Pd particles in Pd coated Cu wire during bonding process were also studied by Zhang *et al.* [37], and discovered that coating Cu wire with palladium prevent Cu from oxidation, meanwhile, at first bonds, the shear stress reduces. Oyinbo and Jen [38,39]studied the effect of surface roughness and temperature on the bonding mechanism between the palladium cluster and copper substrate. They found out that substrate surface configurations have a significant impact on the process of deposition and deformation of the impacting clusters. Also, the palladium-copper interface obtained in their analysis shows a very good mechanical characteristic of approximately (0.70, 0.87, 0.96 and 1.06) GPa tensile strength at (300, 450, 550 and 650) K.

It has also been discovered experimentally that during the cold spray deposition process, adhesion only occurs when the specific sprayed material initial velocity exceeds its critical velocity [2]. The critical velocity for copper particles with sizes between 5-25 μm is about 570 m/s [14]. An experimental analysis of the velocity of particles and the deposition performance in the CGDS process with 20 μm Cu powder on an Al substrate with 640 m/s velocity has established that the particle critical velocity decreases by increasing the particle size, which resulted from strain hardening effect and heat conduction [24]. Studies with stand-off distance variations of copper, titanium and aluminium particles between 10 to 110 mm have shown that a

stand-off distance of 30 mm ensures the greatest possible copper deposition efficiency while aluminium and titanium deposition efficiency decreases as the distances increase [25,40,41].

Therefore, this study focuses on an MD model of CGDS between Pd-Cu (CMM). At the interfacial zone, the plastic deformation behaviours and the process of bonding were examined, and the prevalent determinants of the deformation process discussed. The findings suggest that the deformation process is promoted by shear plastic deformation and a high shear strain rate at the interfacial zone.

2.0 **Material and MD Simulation Methods**

The interfacial deformation and bonding mechanism of Pd-Cu CMM using cold gas dynamic spray process were studied using the Large-scale atomic/molecular massively parallel simulator (LAMMPS) package [42]. For visualizing and analysing atomistic simulation data, open visualization tool (OVITO) [43] and coordination analysis [44–46] were adopted. The Cai and Ye embedded atomic method (EAM) [47] as described below have been used in all the computations of the atomic Interactions.

$$E_i = F\alpha\left(\sum_{j\neq i}\rho_\beta(r_{ij})\right)+\frac{1}{2}\sum_{j\neq i}\Phi\alpha\beta r_{ij} \quad (1)$$

$$\rho_i = \sum_j f\left(r_{ij}\right) \quad (2)$$

Here, the atoms in the model are labelled i and j where $(j \neq i)$. r_{ij} and ρ_β are the distance and electron density respectively between the atom i and j in the solid. The density, ρ_i is the summation of individual atomic densities, $f\left(r_{ij}\right)$ with respect to atom i. The potential function is

denoted by $\Phi\alpha\beta$, and the embedding function, F is the energy that is needed to move atom i into the electron cloud of type α.

In Fig. 1, the initial model configuration of a copper layer (bottom) and a spherical palladium cluster (up). The dimension was set to 30.5nm x 10.85nm x 9.5nm for Cu and 5nm diameter for spherical Palladium cluster and the lattice constants of fcc structured Pd is 0.389 nm and fcc structured Cu is 0.362 nm. The contact surface (x y) of Cu are in (1 0 0) plane orientation. The interfacial region between the materials was not completely smooth. It has been experimentally shown that the material surface roughness has an indirect effect on the bonding process. The surface roughness as shown in Fig 1c displayed the surface unevenness in this study. The wavelength was set to 2.5 nm (1/12 of the Cu layer length) and the maximum displacement was set to 1 nm. Table 1 explains the simulation conditions for the study. As shown in Figure 1d, the substrate is divided into three regions: (a) the top of the substrate consisting of the surface that is exposed directly to particulate effects and containing several atomic layers below it; and (b) the middle bulk region containing several atomic layers that could be maintain during simulations, which are therefore used in thermostatic under the conditions of constant temperature; (c) the bottom of the substrate, a pseudo surface formed by six atomic layers of immobile atoms, which prevents the substrate to be rigidly displaced due to the particle impact. To prevent interaction between the nanoparticle and substrate, the particle was positioned 2 nm over the Cu layer surface. In order to increase simulation measurement performance, the cut-off distance was adopted. For each atom, Verlet algorithm was used to integrate the Newton motion equation [48] Eq. (1)-(3). One femtosecond (1fs) integration timestep was taken. For minimizing energy levels at zero temperatures the system underwent an energy minimization for 0.1 ns. The Nosé Hoover thermostat [49] was used to stabilize the minimum temperature of 300K close to the base of the

copper rigid layers in thermostatic zones both for the substrate and particle for 0.2 ns using NVT ensemble. All other atoms were free to move before the actual deposition of the particle. Figure 1(b) shows the sample equilibrated configuration where the substrate and cluster were set to be fixed. Along x and y direction, Periodic boundary conditions were implemented, while the non-periodic boundary condition was set in the z-direction. The initial particle velocity of 500 m/s, 700 m/s and 1000 m/s was set after equilibration in the z-direction. For deformation and bonding to occur, this initial velocity should be greater than the critical velocity of copper and below particle erosion velocity [50]. The study carried out by Goel *et al*. [34] with varying initial temperature revealed that the velocity used in this analysis is less than the velocity of which particle melting is anticipated to occur. This CGDS deposition process takes place in the NVE ensemble. The molecular dynamics simulation of particle impact in this study was taken to be a process of adiabatic. The radial distribution function (RDF) values were determined based on atomistic data in the above-drift thermostat line in Fig. 1(d).

The Verlet algorithm [48] was used to integrate the Newton motion equation. Using the formula in Eq. 3, the Velocity Verlet-algorithm updates the positions after each timestep Δt

$$r_i(t\ +\Delta t) =\ r_i(t) + v_i(t)\Delta t + \frac{1}{2}a_i(t)\Delta t^2 \tag{3}$$

where

$$v_i(t\ +\Delta t) =\ v_i(t) + \frac{1}{2}[a_i(t) +\ a_i(t\ +\Delta t)]\Delta t \tag{4}$$

The particle acceleration, following Newton's law, can be calculated at time t using Eq. 5

$$a_i(t) = \frac{F_i[r_i(t)]}{m} \tag{5}$$

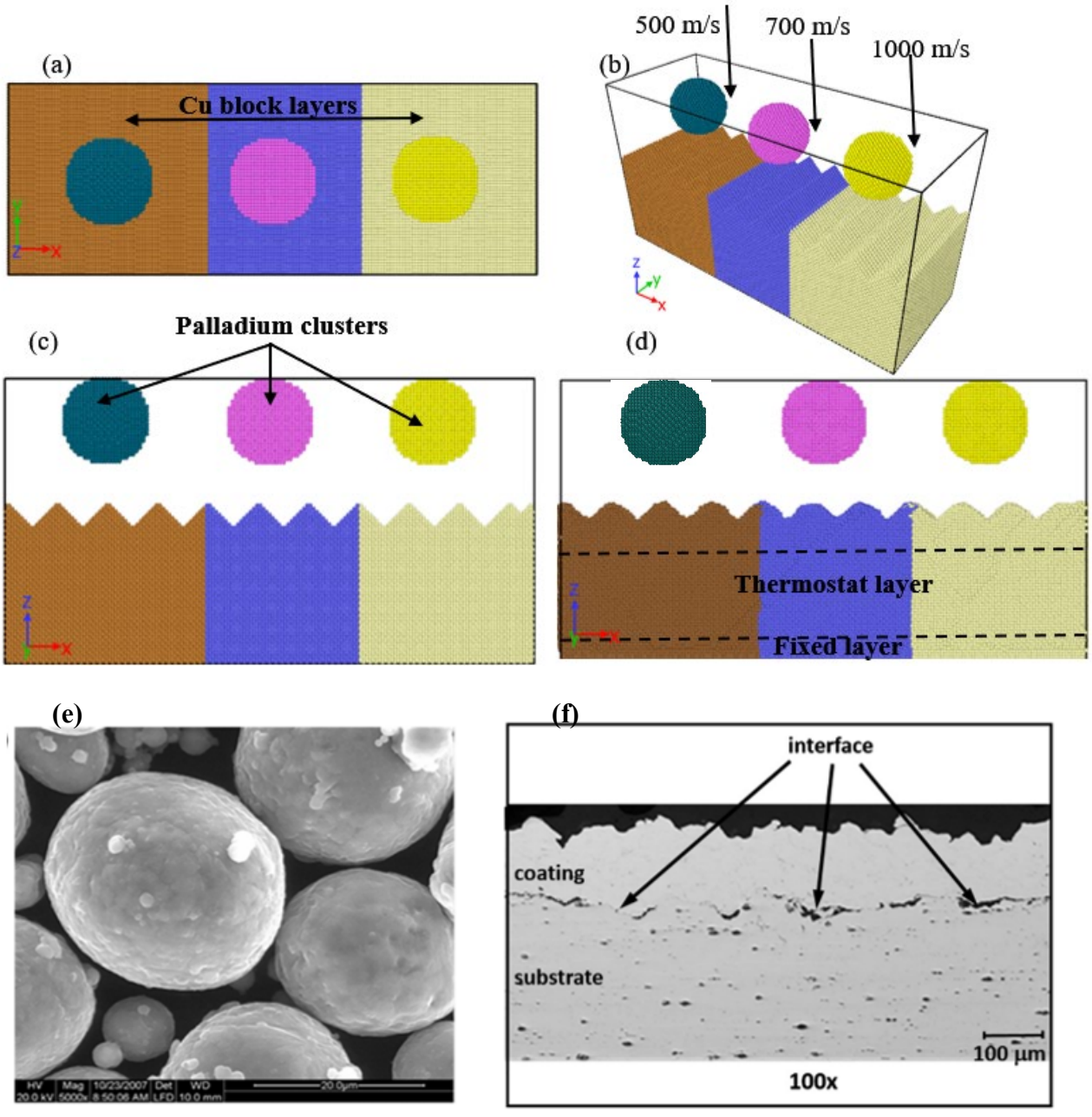
(a)
Cu block layers
(b)
500 m/s
700 m/s
1000 m/s
(c)
Palladium clusters
(d)
Thermostat layer
Fixed layer
(e)
(f)
interface
coating
substrate
100 µm
100x

Fig. 1:Ssnapshot of the simulation model : (a) Plan view configuration of sample (a) Perspective view showing the velocity of the impacting palladium cluster (c) front view configuration of the sample (d) Equilibrated configuration at 300 K for 0.2ns (e) SEM surface [51] (f) Morphology of coating/interface by the microstructure of the coating optical micrograph [51]

Table 1: Schematic MD simulation calculation plan

Materials	Cluster	spherical Pd cluster (diameter 5 nm), 4508 atoms
	Substrate	rectangular Cu 30.5nm x 10.85nm x 9.5nm approx., 301,816 atoms
Operating conditions	duration of simulation	50 ps
	Timestep	1 fs (0.001 ps)
	Number of steps	50,000
	Particle diameter	5 nm
	Impact velocity	500 m/s, 700 m/s, 1000 m/s
	Angle of impact	90°
	Initial Stand-off distance	2 nm
	Boundary condition	p p s
	Potential used	Embedded-atom-method (EAM) [47]
	Initial temperature	300 K
	Substrate Crystal Orientation	1 0 0
	Ensemble	NVT for equilibration, NVE for

3.0 Results and discussion

3.1 Interfacial Structure and deformation Behavior

The atomic configuration at the interface of Pd-Cu CMM is captured in Fig. 2(a)-(d) at impact time histories of 5, 10, 25, and 50 ps to describe the evolution of interfacial deformation behaviour. After the occurrence of excitation, a certain atomic deformation appeared at the interfacial zone, and the interface steadily becomes fuzzy given the number of the limited atoms at this region. Fig. 2a gives a schematic view of the cross-sections at 5 ps showing the fuzzy interfaces. More atoms deform over time so that the Pd-Cu interfaces were gradually expanded into coating zones (Fig. 2b-d). At the coating zone (CZ) there were two boundaries: one bounded by Cu and the other by Pd. The boundaries were indicated CZ-Cu and CZ-Pd borders for convenient discussion.

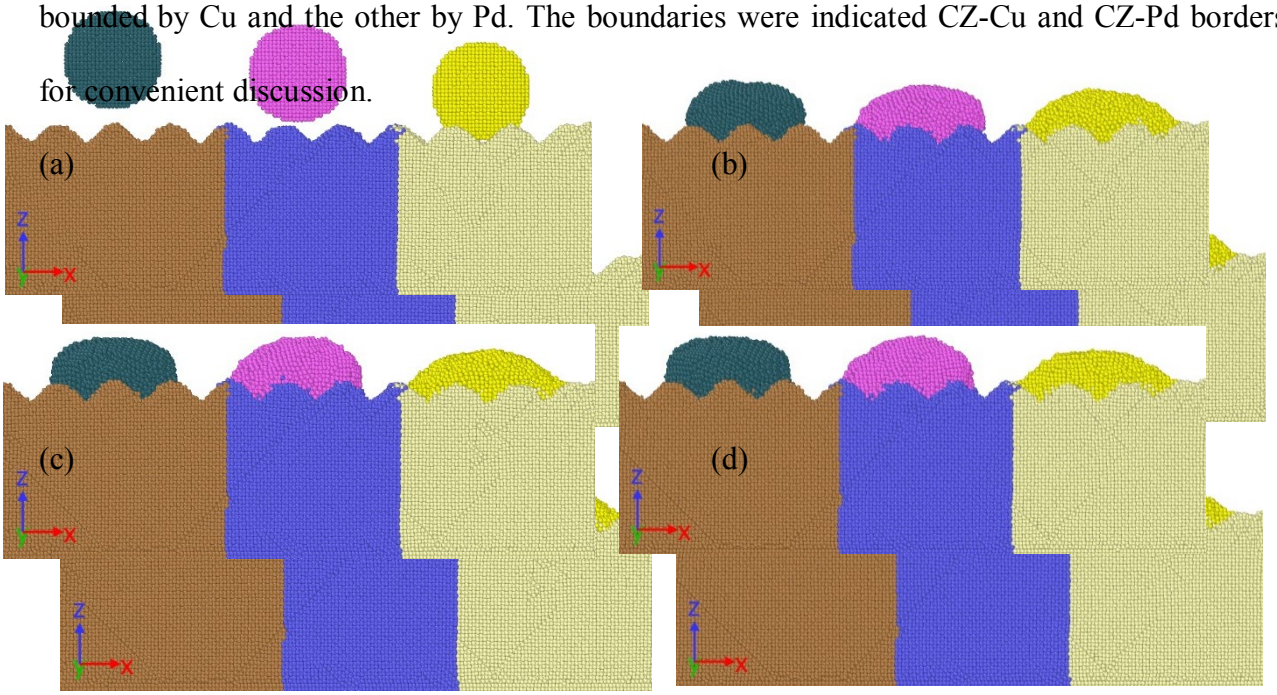

Fig. 2. The schematic view showing the cross-section of the atomic configurations gotten at: (a) 5 ps, (b) 10 ps, (c) 25 ps, and (d) 50 ps. (blue layers: copper block; yellow: palladium cluster at 1000 m/s; purple: palladium cluster at 700 m/s and grey: palladium cluster at 500 m/s)

It is clear that the Pd cluster only has a small number of copper atoms deformed into it, but a high percentage of Pd atoms have deformed into the Cu block. Therefore, it was considerably more rapid to migrate at the CZ-Cu border than the CZ-Pd border, which indicated that asymmetric deformations are present during the coating phase. It is due to the density variance. The density of copper is less than the density of palladium. Therefore, palladium atomic bonds are much stronger than copper ones. The structure for copper fcc was, therefore, easier to break as the palladium cluster deformed essentially into the block. Asymmetric deformation occurs at the Pd-Cu interface during CGDS.

To define the structural transformations, a quantitative ratio between non-fcc structures and fcc structures was used in the composite counterparts (see Fig. 3), the sum of non-fcc structures increased with increasing impact time, and latter decrease due to the gradual rearrangement of the fcc structure at the interfacial zone. MD simulation was also used to analyze stress distribution and the degree of deviatoric deformation during impact at the interfacial region, and Fig. 4 shows the results. The algorithm from Shimzu et al [52] was used to predict the atoms deformation behaviour. A comparison of the atomic configurations using OVITO was carried out for each atom i, which is used to calculate the lagrangian stress matrix given as $\eta_i = {}^1/_2 (JJ_i^T - I)$ with a local deformation matrix J_i. The Von Mises stress was computed for each atom i. The von Mises stress given by η_i^{mises} which measures the ineslastic local deformation and is given in equation

$$\eta_i^{mises} = \sqrt{\eta_{yz}^2 + \eta_{xz}^2 + \eta_{xy}^2 + \frac{\left(\eta_{yy}^2 - \eta_{zz}^2\right) + \left(\eta_{xx}^2 - \eta_{zz}^2\right) + \left(\eta_{xx}^2 - \eta_{yy}^2\right)}{6}} \qquad (6)$$

At the interface of the coating, quite high concentration of stress was observed, mainly due to the pressure and sufficiently rapid impact of high impact velocities resulted in plastic deformation. The interface area has therefore been exposed to complex and high stress, leading to a divergence from the original crystal structures of Cu and Pd atoms and a shift in the order of initial crystal structures into disordered arrangements.

The mechanical energy was converted into strain and heat energy during the process of coating. In turn, both the interfacial stress concentration (Fig. 4) and temperatures in the contact region were increased, which resulted in a deviation from the equilibrium of significant numbers of copper atoms to create instantaneous vacancies. Although some strain energy was emitted with rearranging the interface, some deviated Cu atoms were promoted by the combination with heat energy to migrate to the nearest neighbouring vacancies. That is to say, the Cu block was slightly recovered during the CGDS process. Around the given atom, local atomic density could be described by the radial distribution function, RDF g(r) [53,54]. RDFs have been conducted in the contact zone at a different coating time and the data are compiled at different speeds in Fig. 6 to further explain variations in the molecular structure. During the first phase of deposition, there were small projections in the RDFs, showing the short-ranged and long-ranged order of the crystal-structural properties. The pairs of Pd-Pd and Cu-Cu crystallinity at the interfacial zone subsequently weakened significantly, and characteristics liquid-like nature emerged due to plastic deformation. The fluctuation of RDFs which tended to 0 showed the characteristics of the long-ranged disorder and short-ranged order. On the relaxation point, in the

RDFs, some small peaks took place and the crystal structure again emerged. Therefore, the clusters and the copper at the interfacial zone transform to liquid-like state from the crystal structure state then evolved back into its crystal form after the impact. Fig. 5(a), (c), (e) and Fig. 5(b), (d), (f) indicates some variations in the size of the Cu-Cu pair and Pd-Pd pair peak intensity respectively. Unlike the Cu-Cu g(r) plots, however, the Pd-Pd pair's peak intensity gradually decreased overtime at all velocities. These results further confirmed the recuperation in distorted crystals at low temperatures.

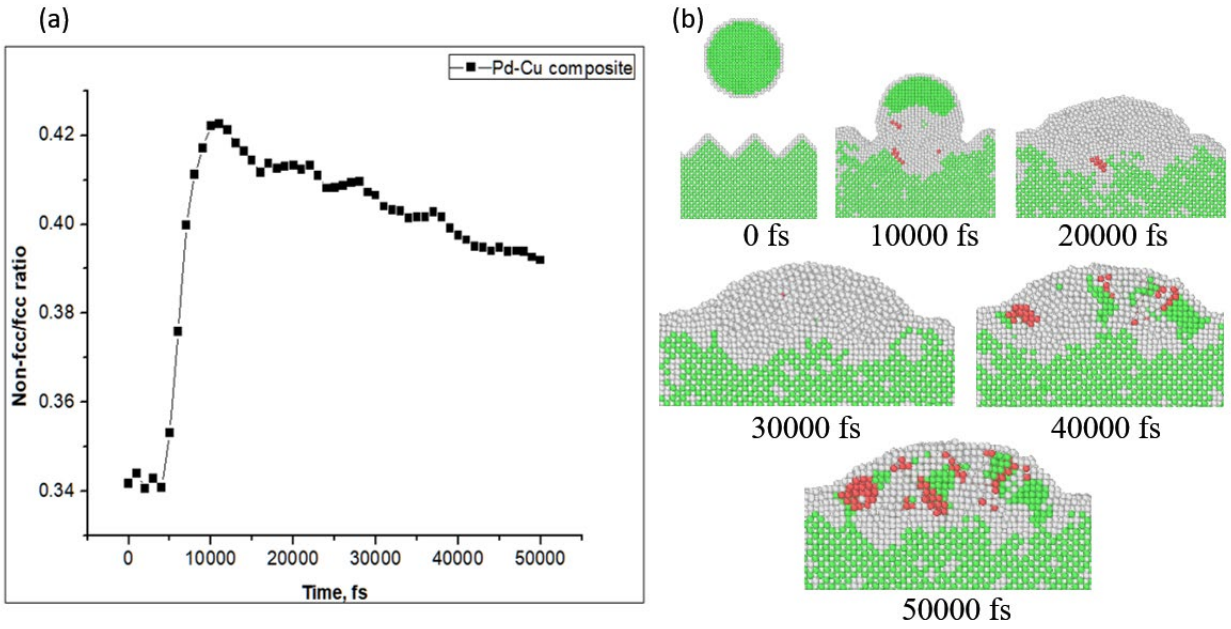

Fig. 3: Structural transformation at the Pd-Cu interfacial zone (a) non-fcc/fcc structures ratio (b) cross-section of Pd-Cu CMM with respect to time (green: fcc structure; grey and red: non-fcc structure)

Fig. 4: Stress distribution of the interfacial zone at: (a)2 ps, (b) 5 ps, and (c) 10 ps : (d) 20 ps, (e) 30 ps, and (f) 50 ps.

(a)

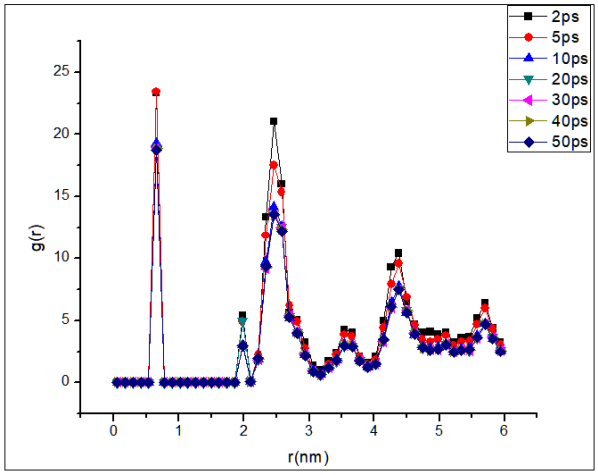

(b)

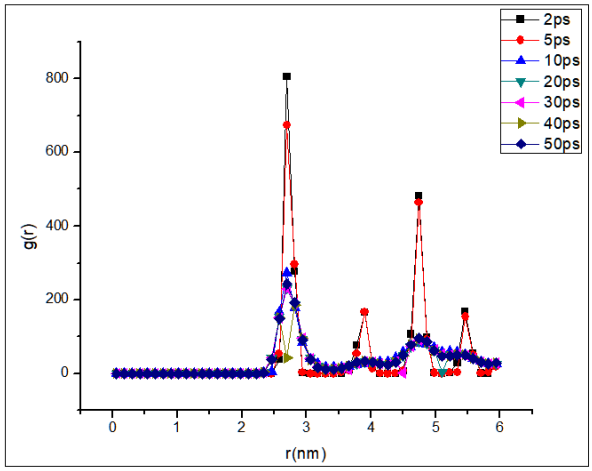

(c)

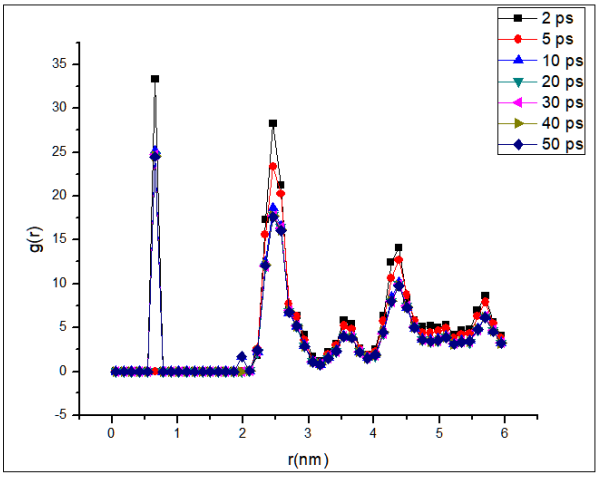

(d)

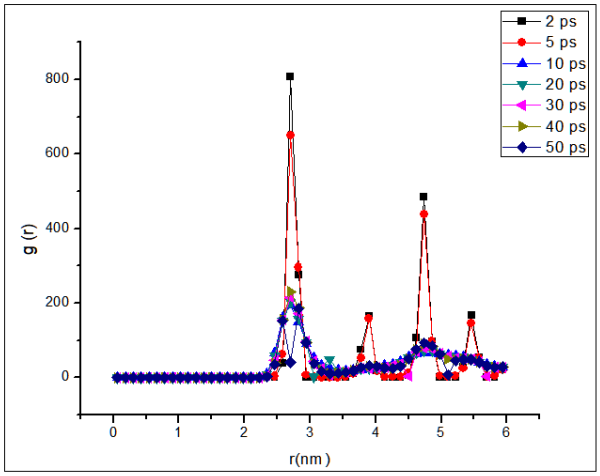

(e) (f)

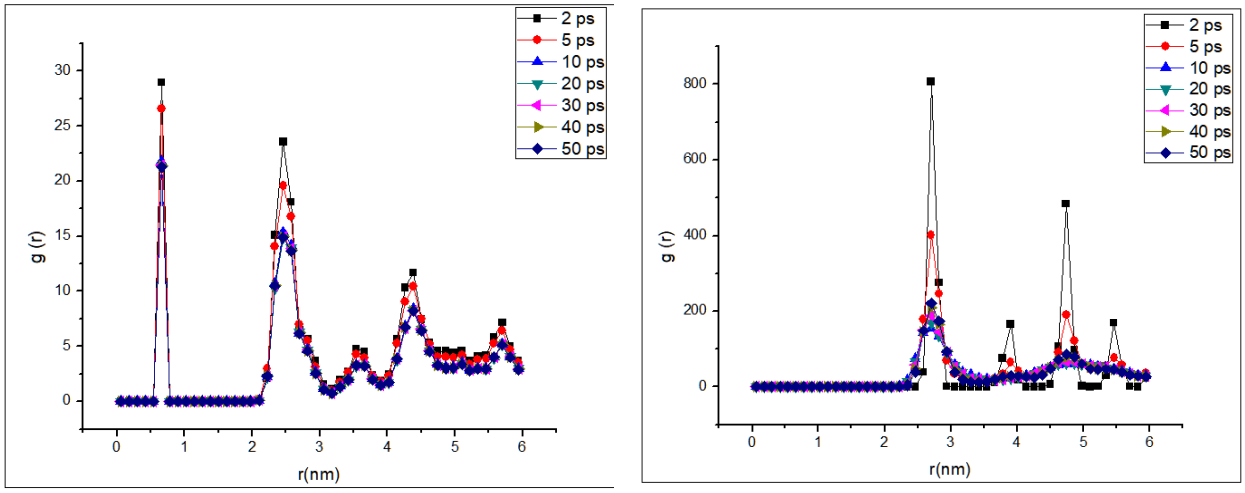

Fig. 5: Fluctuations in radial distribution functions (RDF): (a) Cu–Cu at 500 m/s and (b) Pd–Pd at 500 m/s (c) Cu–Cu at 700 m/s and (d) Pd–Pd at 700 m/s (e) Cu–Cu at 1000 m/s and (f) Pd–Pd at 1000 m/s initial impact velocity.

This CGDS simulations in MD, however, showed that the palladium clusters' temperature was less than 500 K at 1000 m/s initial velocity and 350 K and 380 K at 500 m/s and 700 m/s respectively as shown in Fig. 6. These temperatures, therefore, may not be sufficiently high to disseminate strong state response. The deformation process in CGDS has been accelerated in order to attribute CGDS reaction-deformation to stress, strain and local fusion (thermal effect). Otherwise, metals are usually followed by severe plastic deformation by high strain and large shear deformations. The deformation process was more rapidly accelerated by shear deformation [55,56]. Crystal lattice could quickly crack through shear deformation, while the shear strain energy could surpass the strength of the deformation activation and energy barrier.

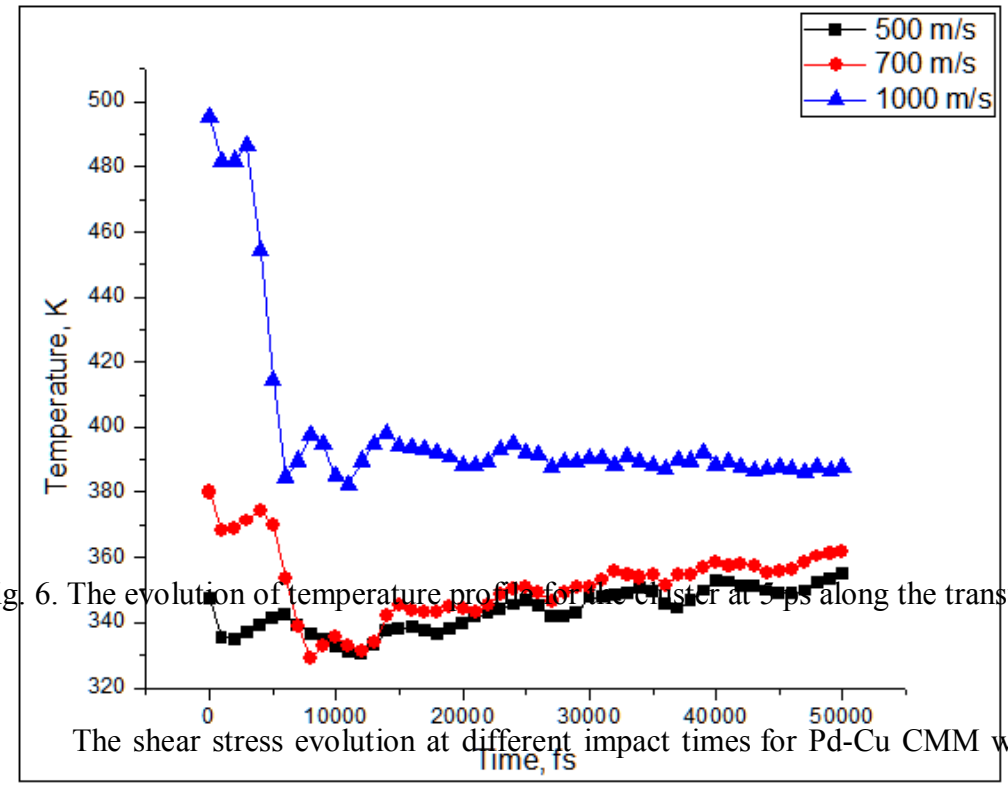

Fig. 6. The evolution of temperature profile for the cluster at 5 ps along the transverse direction.

The shear stress evolution at different impact times for Pd-Cu CMM was extracted and shown in Fig. 7. At the interfacial zone, a progressive shear plastic deformation region was observed, Furthermore, the shear strain changed considerably as the impact time rose. This suggests that the interface area was deformed at higher strain rates. As a consequence, significant numbers of palladium and copper atoms moved to both ends of the neighbouring interface from their original stable positions during the CGDS process. Meanwhile, high instantaneous levels of vacancy concentrations during the coating process have developed. The vacancy concentration could be increased by the high strain rates in Pd up to 7×10^{-2} [57]. The vacancies might perhaps be regarded as the finest equilibrium states for large-scale migration of heterogeneous atoms. Inter- deformation within different atoms could be created if the Pd (or Cu side) vacancies in the Pd-Cu interface were a new Pd atoms (or Cu atoms) equilibrium position. The chemical reaction occurred between Pd and Cu when the concentration of Cu during the deformation

reaches the solid solubility limit, the inter-metallic composite will be produced. The presence of the plateau would, therefore, indicate the transitions caused by deformation during CGDS.

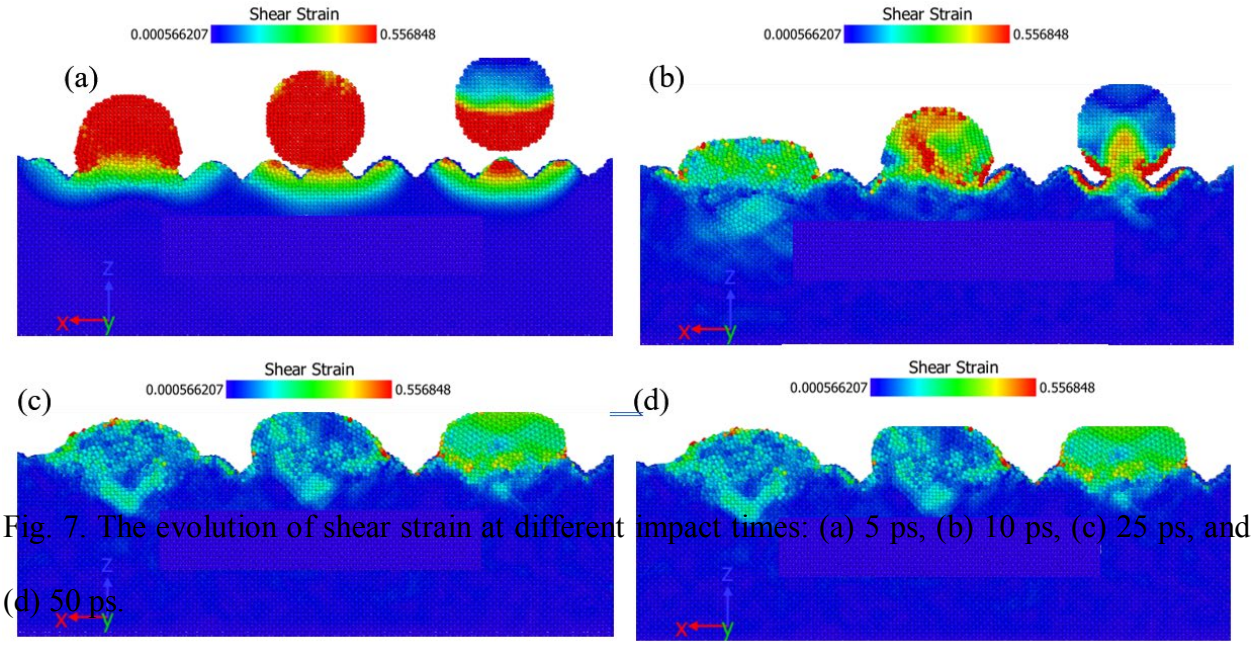

Fig. 7. The evolution of shear strain at different impact times: (a) 5 ps, (b) 10 ps, (c) 25 ps, and (d) 50 ps.

3.2 Force - displacement curves

The visual representation of these atomic simulations enables for explicit evaluation during the computation of atomic configurations within the system of any physical quantity including the forces exerted by each atom that can be calculated. For visualizing and analysing atomistic deformation data, open visualization tool (OVITO) [43] and coordination analysis [44–46] were used. In OVITO, the atomic configurations of each palladium cluster and magnitude of the force exerted on each atom were located before and directly after the sudden fall in the cluster's force. To ensure and capture the occurrence of the transition from elastic to plastic region at a different velocity, three palladium clusters were accelerated towards Cu crystal block to investigate the plastic deformations mechanisms due to high-speed impact. These three palladium clusters experience a large and sudden drop in their force after impact. Fig. 8 shows the force-

displacement curve at different cluster velocity. Due to this high impact velocity, all the three clusters experience force drop suddenly after impact. This section focuses on the initial deformation event to investigate the deformation mechanism during this first sudden force drop at 24 Å for the 500 m/s, 28 Å for 700 m/s and 37 Å for 1000 m/s.

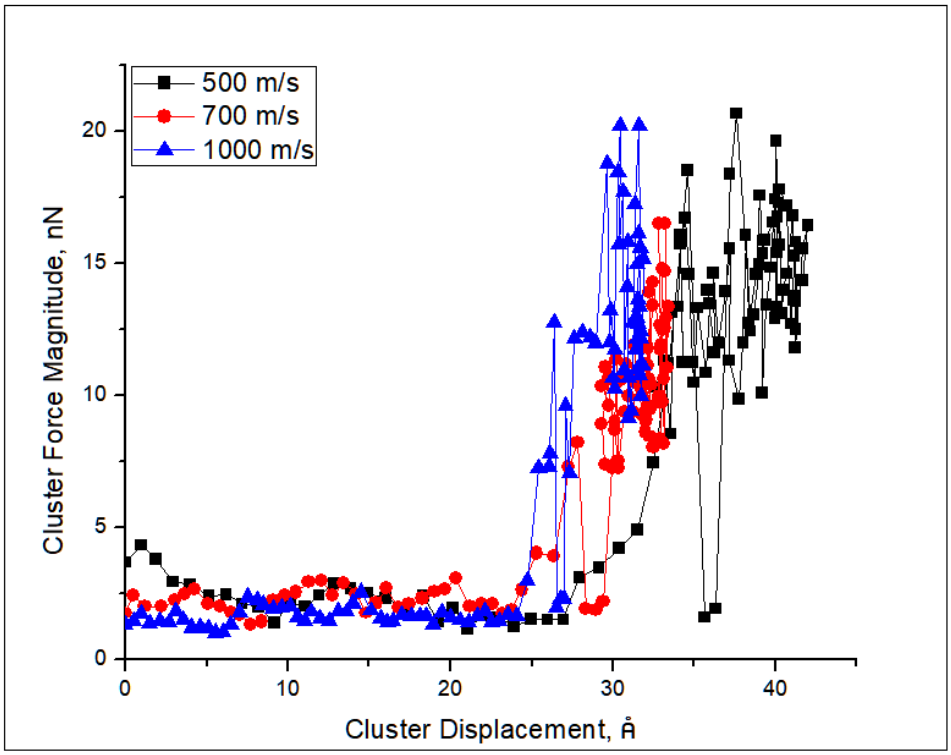

Fig 8: The force – vertical displacement curves with 500 m/s, 700 m/s and 1000 m/s cluster initial velocity.

This simulation of deformation and retraction was conducted to verify that such initial sudden force declines are correlated with permanent plastic failure occurrences. The force magnitude on each palladium cluster was calculated on every displacement as soon as the cluster retracted after it deforms to the depths corresponding to the sudden force drop. It was discovered that the retraction of these clusters atoms at this initial stage makes the cluster force to quickly drop considerably. This implied that the cluster had been separated momentarily from the Cu atoms and that the Cu atoms could not recuperate from the deformation. Consequently, the deformation linked to these abrupt drops of force was the irreversible, energetically stable deformation. Fig. 9 shows the force-displacement curves for the simulations of deformation and retraction for minor force events with 24 Å, 28 Å and 37 Å displacements along z-direction corresponding to the initial force drop. These occurrences reflected elastic mobility of atoms underneath the palladium cluster. The deformation and refraction at these displacements determined this event. The force at each displacement was equal to the corresponding displacement force as the clusters were retracted.

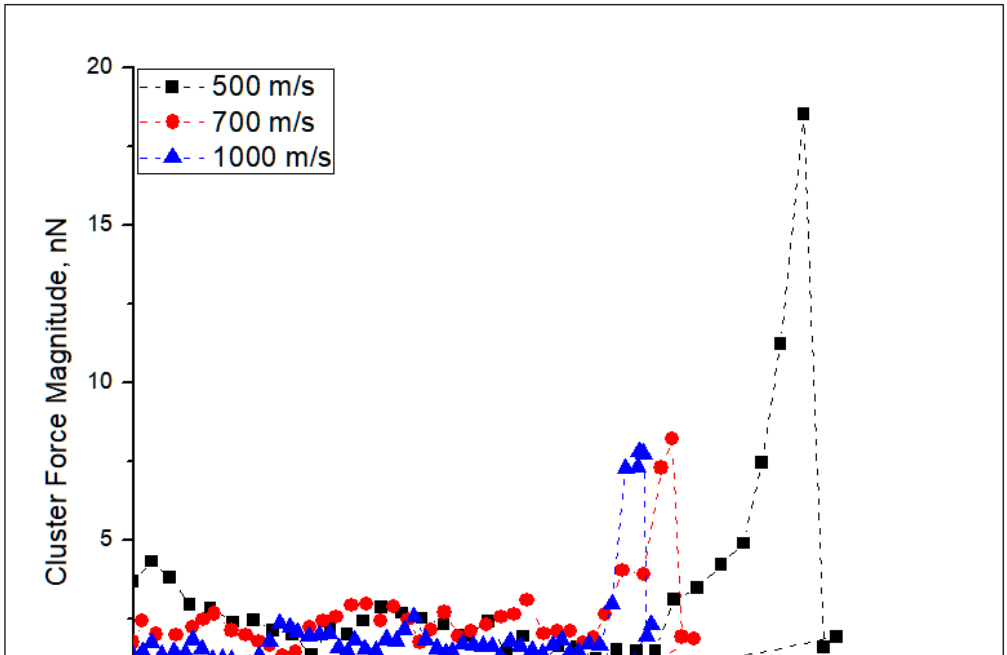

Fig. 9: The force-displacement curves before sudden force drop with 500 m/s, 700 m/s and 1000 m/s cluster initial velocity (The trend of data is shown by the dotted lines, not physical quantities).

The mechanism associated with these plastic events had to be determined because these sudden forces drop initially experienced by palladium clusters were the energetically stable plastic deformations in the Cu layer. As already described, the hypothesized mechanism of deformation was proposed for broken bonds to occur [26,28]. The method adopted in this study was, therefore, to explicitly analyze directly the atomic bond between atoms before and after the event of a sudden drop in the cluster force (transition from elastic to plastic). This was done primarily to establish if the unexpected drop in the cluster force was due to the breaking of bonds between the atoms of copper layers. To do that analysis, the atomic bond of all pairs of atoms in the interfacial zone was computed by the OVITO. The create bonds modifier in OVITO creates bonds between particles using a pair-wise cut-off criterion. The visual appearance of the generated bonds is controlled by the bonds displayed. It was surprisingly noted that no bonds were broken during the initial plastic deformation event (first force drop) in the analysis of the atoms' bonding before and after plastic events (Fig.10). The primary deformation mechanism

related to the initial cluster force drop event has therefore been shown not to be a result of broken bonds. For this initial plastic deformation to occur, stable energetically and permanent another deformation mechanism must be considered. Therefore, the hydrodynamic behaviour between bonded atoms at this initial plastic deformation event resulted from the interaction of surface roughness at the interfacial zone, strong pressure effect from high-velocity impact, and the combination of locking due to Kelvin-Helmholtz instability and local fusion (thermal effect)

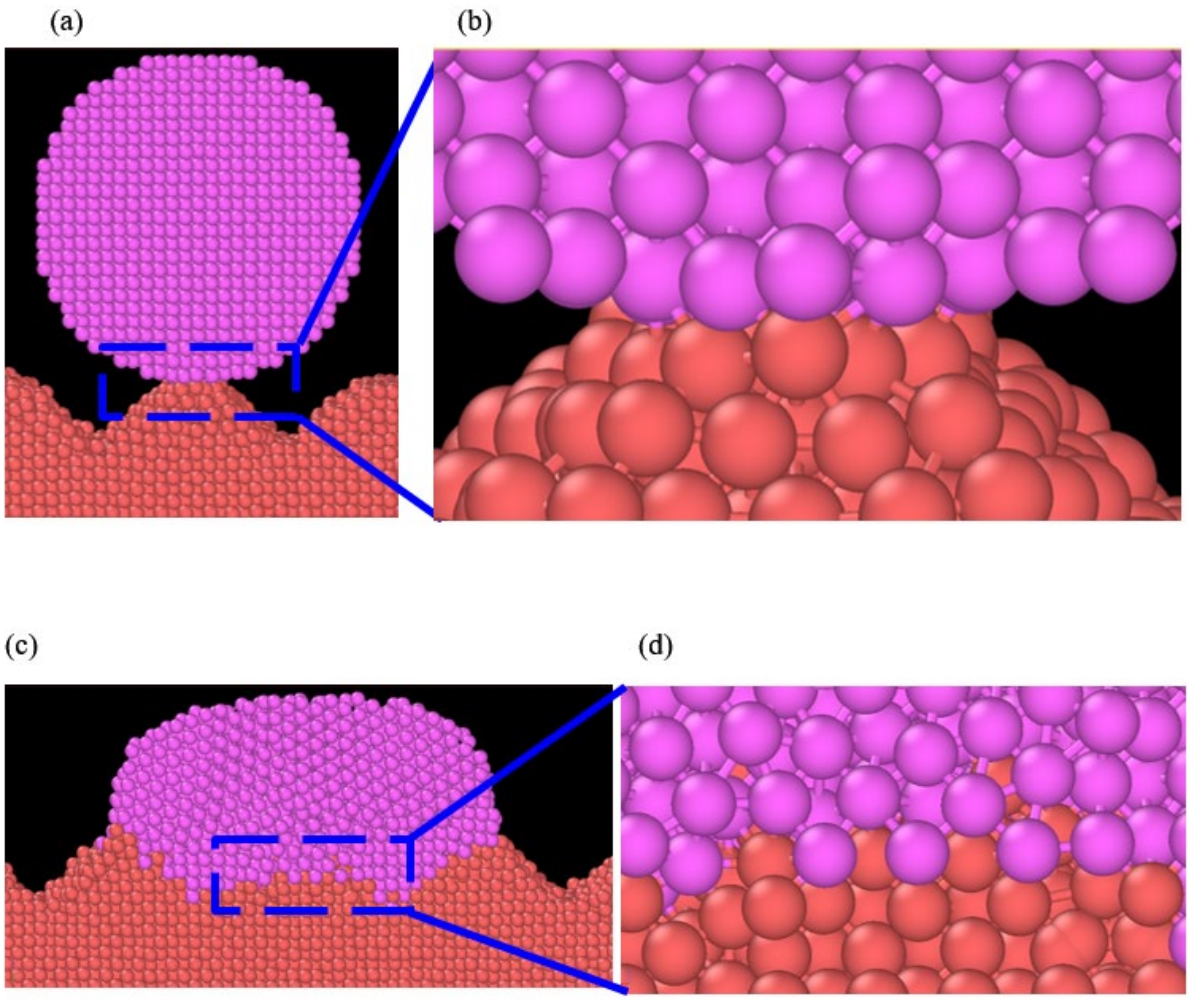

Fig. 10: a snapshot of the bonding mechanism at the interfacial zone with 500 m/s impact velocity and 300 K (a) first contact view at 7 ps (b) magnified view of the first contact (c) contact view at 50 ps (d) magnified view of the contact at 50 ps

3.3 Interfacial Bonding Strength at a different initial impact velocity

The interface bond energy demonstrated bonding strength and compatibility between the Cu substrate and Pd clusters. The Pd-Cu CMM interface bond energy can be described with interfacial bonding strength (IBS) and interfacial shearing strength (ISS). The compatibility and interface strength of the composite materials resulted from the higher binding energy. The

following described the method of calculating interfacial bonding energy [58]. The total energy of the molecular system (E_T) is the addition of the potential energy ($E_{potential}$) of the system and the kinetic energy ($E_{kinetic}$). The summation of intermolecular potential energy, potential energy and interaction energy gives the molecular potential energy. The intermolecular potential energy ($E_{non-bond}$) includes hydrogen binding energy ($E_{hydrogen\ bond}$), Van der Waals energy ($E_{van\ dar\ waals}$), and electrostatic energy ($E_{electrostatic}$).

$$E_T = E_{kinetic} + E_{potential} \tag{7}$$

$$E_{non-bond} = E_{van\ dar\ waals} + E_{electrostatic} + E_{hydrogen\ bond} \tag{8}$$

At different impact velocity for Pd-Cu CMM, the interfacial bonding energy is given by Eq. 9 [39]:

$$E_{inter\ face} = E_T - (E_{Pd} + E_{Cu}) \tag{9}$$

where E_T, E_{Pd} and E_{Cu} are the potential energy of Pd-Cu CMM, Pd cluster and Cu respectively.

Another way of characterizing interfacial bonding energy is the interfacial shearing strength. Interfacial shearing strength which is the energy required for the total extraction of the nanomaterials from the composites can be deduce $E_{pullout}$. This energy is equal in magnitude to $E_{inter\ face}$. Eq. 10 and Eq. 11 can be used to calculate the interfacial shearing energy [59].

$$E_{pullout} = \left|E_{inter\ face}\right| = \int_{x=0}^{x=1} A\tau_i dz = \int_{x=0}^{x=1} 2S\tau_i dz = \int_{z=0}^{z=1} 2h(L-x)\tau_i dz = h\tau_i L^2 \tag{10}$$

$$\tau_i = \frac{\left|E_{inter\ face}\right|}{hL^2} \tag{11}$$

Where L, h and S are the length, width and cross-section area of the palladium cluster, respectively. The drawing direction coordinate is denoted by z. τ_i is the shear stress.

As Table 2 shows, each model's potential energy values were measured for 50 ps at its equilibrium process. Hence, Pd-Cu CMMs' potential energy is substantially greater than that of pure Cu. The negative values of interfacial bonding energy indicated higher interaction between the Pd cluster and the Cu substrate. Fig. 11 shows the calculated Pd-Cu CMM' interface bonding energy with different initial impact velocities at 50 ps impact time. From these results, the calculated interfacial bonding energy for Pd-Cu CMM at 500 m/s, 700 m/s and 1000 m/s are found to be -1346.56 kcal/mol, -1343.28 kcal/mol, and -1244.3 kcal/mol respectively and the interfacial shearing strength corresponding to these velocities are 27.5 MPa, 27.26 MPa, and 25.3 MPa. In other words, there is no significant difference in the interfacial strength of Pd-Cu CMM for 500 m/s and 700 m/s. Furthermore, the higher interfacial bonding energy and interfacial shearing strength value of the interface at 500 m/s and 700 m/s implies that the interfacial bonding strength between Pd and Cu is larger so that the region of impact on Cu surface is more compact within a certain range after impact

Table 2: The Pd-Cu CMM interaction energy

Velocity	E_{Pd} $KCal/mol$	E_{Cu} $KCal/mol$	E_T $KCal/mol$	$E_{Inter\ face}$ $KCal/mol$
500 m/s	1289.62	3580.76	3523.62	-1346.56
700 m/s	3447.8	1275.62	3515.47	-1343.28
1000 m/s	3499.78	1192.92	3551.25	-1244.39

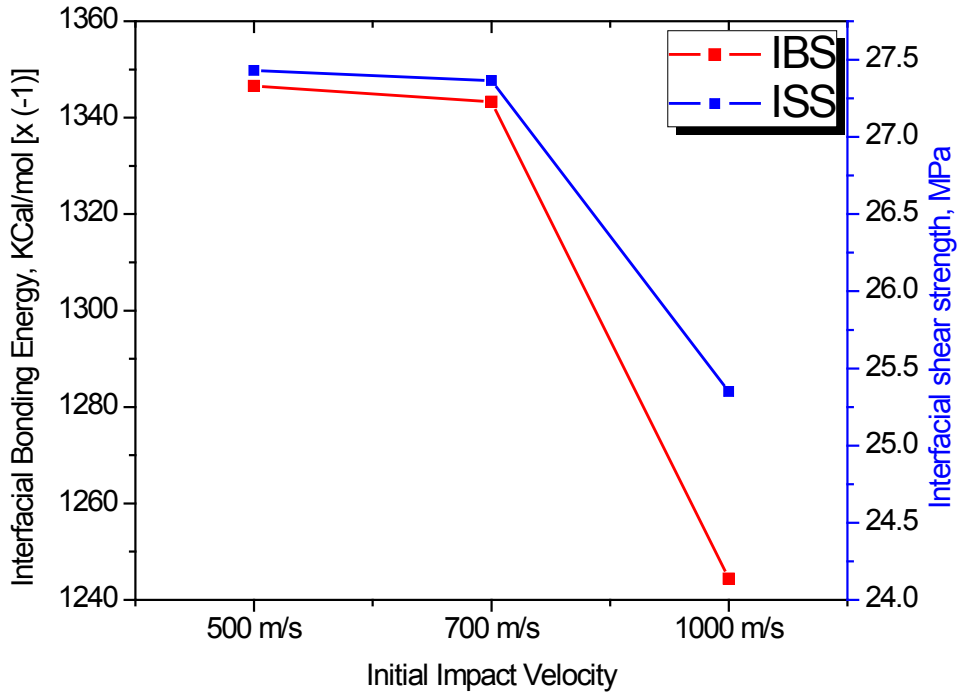

Fig. 11: The interfacial binding energy of Pd-Cu CMM

4. Conclusions

Molecular dynamic simulations were used to explore the atomic deformation behaviours and bonding mechanism at the interfacial zone of Pd-Cu CMM during CGDS. The following are the conclusions of the study:

1. The variation in the concentration of Pd and that of Cu caused the Pd front to migrate with much faster velocity than the Cu front, and the interfacial zone between Pd and Cu experiences asymmetric deformation during CGDS.
2. During the CGDS process, the region of the interface was subjected to complex and high stress, turning the perfect fcc-structures of Cu into a chaotic configuration, increasing the non-fcc-structures number over time.
3. The RDF peak intensity gradually decreased overtime at all velocities as the impact time increases. These results confirmed the recuperation in distorted crystals at low temperatures during the coating process.
4. The deformation during the CGDS is an unsteady and dynamic process. The deformation during this process is mainly due to elevated shear strain rate and shear plastic deformation at the interface of the contact region.
5. From this study, it was shown using force-displacement curves that the primary deformation mechanism related to the initial force drop event of the palladium cluster has therefore been shown not to be a result of broken bonds. For this initial plastic deformation to occur, stable energetically and permanent another deformation mechanism must be considered. Therefore, the hydrodynamic behaviour between bonded atoms at this initial plastic deformation event resulted from the interaction of surface roughness at the interfacial zone, strong pressure effect from high-velocity impact, and the

combination of locking due to Kelvin-Helmholtz instability and local fusion (thermal effect)

6. The higher interfacial bonding energy and interfacial shearing strength value of the interface at 500 m/s and 700 m/s implies that the interfacial bonding strength between Pd and Cu is larger so that the region of impact on Cu surface is more compact within a certain range after impact

Acknowledgement

The authors would like to acknowledge the financial support from the University Research Committee of the University of Johannesburg and the National Research Foundation of South Africa

Declaration of Competing Interest

The authors declare that they have no known competing financial interests or personal relationships that could have appeared to influence the work reported in this paper.

Reference

[1] A.P. Alkhimov, A.N. Papyrin, V.F. Kosarev, N.I. Nesterovich, M.M. Shushpanov, Gas-dynamic spraying method for applying a coating, In, Google Patents. (1994).

[2] T. Klassen, H. Assadi, H. Kreye, F. G, Cold spraying - A materials perspective, Acta Mater. 116 (2016) 382–407. https://doi.org/10.1016/j.actamat.2016.06.034.

[3] M. Grujicic, J.R. Saylor, D.E. Beasley, W.S. DeRosset, D. Helfritch, Computational

analysis of the interfacial bonding between feed-powder particles and the substrate in the cold-gas dynamic-spray process, Appl. Surf. Sci. 219 (2003) 211–227. https://doi.org/10.1016/S0169-4332(03)00643-3.

[4] Y. Chang, P. Mohanty, N. Karmarkar, M. Tahir, Y. Wang, J. Wang, Microstructure and properties of Cu – Cr coatings deposited by cold spraying, Vacuum. 171 (2020) 109032. https://doi.org/10.1016/j.vacuum.2019.109032.

[5] A. Moridi, S.M. Hassani-Gangaraj, M. Guagliano, M. Dao, Cold spray coating: Review of material systems and future perspectives, Surf. Eng. 30 (2014) 369–395. https://doi.org/10.1179/1743294414Y.0000000270.

[6] R.N. Raoelison, C. Verdy, H. Liao, Cold gas dynamic spray additive manufacturing today: Deposit possibilities, technological solutions and viable applications, Mater. Des. 133 (2017) 266–287. https://doi.org/10.1016/j.matdes.2017.07.067.

[7] R.N. Raoelison, Y. Xie, T. Sapanathan, M.P. Planche, R. Kromer, S. Costil, C. Langlade, Cold gas dynamic spray technology : A comprehensive review of processing conditions for various technological developments till to date, Addit. Manuf. 19 (2018) 134–159. https://doi.org/10.1016/j.addma.2017.07.001.

[8] Y.-Y. Wang, L. Yi, C.-X. Li, G.-J. Yang, Y. Liu, C.-J. Li, G.-J. Yang, K. Kusumoto, Electrical and mechanical properties of nano-structured TiN coatings deposited by vacuum cold spray, Vaccum. 86 (2012) 953–959. https://doi.org/10.1016/j.vacuum.2011.06.026.

[9] S.T. Oyinbo, T.-C. Jen, A comparative review on cold gas dynamic spraying processes and technologies, Manuf. Rev. (2019) 11–13. https://doi.org/10.1051/mfreview/2019023.

[10] S.R. Vadla, Simulation of Gas Dynamic Cold Spray Process, Electron. Theses Diss.

(2018) 2680. https://doi.org/https://openprairie.sdstate.edu/etd/2680 This.

[11] S. Pathak, G. Saha, Development of Sustainable Cold Spray Coatings and 3D Additive Manufacturing Components for Repair/Manufacturing Applications: A Critical Review, Coatings. 7 (2017) 122. https://doi.org/10.3390/coatings7080122.

[12] W.-Y. Li, H. Liao, C.-J. Li, H.-S. Bang, C. Coddet, Numerical simulation of deformation behavior of Al particles impacting on Al substrate and effect of surface oxide films on interfacial bonding in cold spraying, Appl. Surf. Sci. 253 (2007) 5084–5091. https://doi.org/10.1016/j.apsusc.2006.11.020.

[13] S. Singh, H. Singh, Effect of electroplated interlayers on bonding mechanism of cold-sprayed copper on SS316L steel substrate, Vacuum. 172 (2020) 109092. https://doi.org/10.1016/j.vacuum.2019.109092.

[14] J. Vlcek, L. Gimeno, H. Huber, E. Lugscheider, A Systematic Approach to Material Eligibility for the Cold-Spray Process, J. Therm. Spray Technol. 14 (2005) 125–133. https://doi.org/10.1361/10599630522738.

[15] S. Yin, X. Wang, W. Li, H. Liao, H. Jie, Deformation behavior of the oxide film on the surface of cold sprayed powder particle, Appl. Surf. Sci. 259 (2012) 294–300. https://doi.org/10.1016/j.apsusc.2012.07.036.

[16] S. Yin, X.-F. Wang, W.Y. Li, H.-E. Jie, Effect of substrate hardness on the deformation behavior of subsequently incident particles in cold spraying, Appl. Surf. Sci. 257 (2011) 7560–7565. https://doi.org/10.1016/j.apsusc.2011.03.126.

[17] H. Takana, K. Ogawa, T. Shoji, H. Nishiyama, Computational simulation of cold spray process assisted by electrostatic force, Powder Technol. 185 (2008) 116–123. https://doi.org/10.1016/j.powtec.2007.10.005.

[18] S. Rahmati, A. Zúñiga, B. Jodoin, R.G.A. Veiga, Deformation of copper particles upon impact: A molecular dynamics study of cold spray, Comput. Mater. Sci. 171 (2020) 109219. https://doi.org/10.1016/j.commatsci.2019.109219.

[19] D. Alamanova, V.G. Grigoryan, M. Springborg, Deposition of copper clusters on the Cu (1 1 1) surface, Surf. Sci. 602 (2008) 1413–1422. https://doi.org/10.1016/j.susc.2008.02.002.

[20] H. Gao, L. Zhao, D. Zeng, L. Gao, Molecular Dynamics Simulation of Au Cluster Depositing on Au Surface in Cold Gas Spray, in: First Int. Conf. Integr. Commer. Micro Nanosyst. Parts A B, 2007: pp. 1–8. https://doi.org/10.1115/mnc2007-21609.

[21] S.T. Oyinbo, T.C. Jen, Investigation of the process parameters and restitution coefficient of ductile materials during cold gas dynamic spray (CGDS) using finite element analysis, Addit. Manuf. 31 (2020) 100986. https://doi.org/10.1016/j.addma.2019.100986.

[22] F. Khodabakhshi, B. Marzbanrad, H. Jahed, A.P. Gerlich, Interfacial bonding mechanisms between aluminum and titanium during cold gas spraying followed by friction-stir modi fi cation, Appl. Surf. Sci. 462 (2018) 739–752. https://doi.org/10.1016/j.apsusc.2018.08.156.

[23] R. Nikbakht, S.H. Seyedein, S. Kheirandish, H. Assadi, B. Jodoin, Asymmetrical bonding in cold spraying of dissimilar materials, Appl. Surf. Sci. 444 (2018) 621–632. https://doi.org/10.1016/j.apsusc.2018.03.103.

[24] T. Schmidt, F. Gärtner, H. Assadi, H. Kreye, Development of a generalized parameter window for cold spray deposition, Acta Mater. 54 (2006) 729–742. https://doi.org/10.1016/j.actamat.2005.10.005.

[25] K. Alamara, S. Saber-samandari, C.C. Berndt, Splat taxonomy of polymeric thermal spray coating, Surf. Coat. Technol. 205 (2011) 5028–5034.

https://doi.org/10.1016/j.surfcoat.2011.05.002.

[26] M. Grujicic, C.. Zhao, W.. DeRosset, D. Helfritch, Adiabatic shear instability based mechanism for particles/substrate bonding in the cold-gas dynamic-spray process, Mater. Des. 25 (2004) 681–688. https://doi.org/10.1016/j.matdes.2004.03.008.

[27] G. Bae, Y. Xiong, S. Kumar, K. Kang, C. Lee, General aspects of interface bonding in kinetic sprayed coatings, Acta Mater. 56 (2008) 4858–4868. https://doi.org/10.1016/j.actamat.2008.06.003.

[28] H. Assadi, F. Gärtner, T. Stoltenhoff, H. Kreye, Bonding mechanism in cold gas spraying, Acta Mater. 51 (2003) 4379–4394. https://doi.org/10.1016/S1359-6454(03)00274-X.

[29] Y. Xie, S. Yin, C. Chen, M.-P. Planche, H. Liao, R. Lupoi, New insights into the coating/substrate interfacial bonding mechanism in cold spray, Scr. Mater. 125 (2016) 1–4. https://doi.org/10.1016/j.scriptamat.2016.07.024.

[30] M. Hassani-Gangaraj, D. Veysset, V.K. Champagne, K.A. Nelson, C.A. Schuh, Adiabatic shear instability is not necessary for adhesion in cold spray, Acta Mater. 158 (2018) 430–439. https://doi.org/10.1016/j.actamat.2018.07.065.

[31] S.T. Oyinbo, T. Jen, Feasibility of numerical simulation methods on the Cold Gas Dynamic Spray (CGDS) Deposition process for ductile materials, Manuf. Rev. 7 (2020) 1–15. https://doi.org/10.1051/mfreview/2020023.

[32] A. Joshi, S. James, Molecular Dynamics Simulation Study on Effect of Process Parameters on Coatings during Cold Spray Process, Procedia Manuf. 26 (2018) 190–197. https://doi.org/10.1016/j.promfg.2018.07.026.

[33] T. Malama, A. Hamweendo, I. Botef, Molecular Dynamics Simulation of Ti and Ni Particles on Ti Substrate in the Molecular Dynamics Simulation of Ti and Ni Particles on

Ti Substrate in the Cold Gas Dynamic Spray (CGDS) Process, Process. Mater. Sci. Forum. 828–829 (2015) 453–460. https://doi.org/10.4028/www.scientific.net/MSF.828-829.453.

[34] S. Goel, N. Haque, V. Ratia, A. Agrawal, A. Stukowski, Atomistic investigation on the structure – property relationship during thermal spray nanoparticle impact, Comput. Mater. Sci. 84 (2014) 163–174. https://doi.org/10.1016/j.commatsci.2013.12.011.

[35] M.I. Rojas, M.G. Del Po, E.P.M. Leiva, Simulation Study of Pd Submonolayer Films on Au (hkl) and Pt (hkl) and Their Relationship to Underpotential Deposition, Langmuir. 16 (2000) 9539–9546. https://doi.org/10.1021/la990731g.

[36] X. Guo, B. Zhong, P. Brault, Growth and ripening of two-dimensional palladium islands on Ni (111) surface, Surf. Sci. 409 (1998) 452–457. https://doi.org/10.1016/s0039-6028(98)00243-x.

[37] B. Zhang, K. Qian, T. Wang, Y. Cong, M. Zhao, X. Fan, J. Wang, Behaviors of Palladium in Palladium coated copper wire bonding process, 2009 Int. Conf. Electron. Packag. Technol. High Density Packag. ICEPT-HDP 2009. (2009) 662–665. https://doi.org/10.1109/ICEPT.2009.5270668.

[38] S.T. Oyinbo, T.-C. Jen, Y. Zhu, O.O. Abegunde, S. Aasa, Development of Palladium Nanoparticles deposition on a Copper substrate using a Molecular Dynamic (MD) simulation: A Cold Gas Dynamic spray process, Manuf. Rev. 7 (2020) 1–15. https://doi.org/10.1051/mfreview/2020028.

[39] S.T. Oyinbo, T. Jen, Molecular dynamics investigation of temperature effect and surface configurations on multiple impacts plastic deformation in a palladiumcopper composite metal membrane (CMM): A cold gas dynamic spray (CGDS) process, Comput. Mater.

Sci. 185 (2020) 109968. https://doi.org/https://doi.org/10.1016/j.commatsci.2020.109968.

[40] V. Pershin, S. Chandra, J. Mostaghimi, Splat Shapes in a Thermal Spray Coating Process : Simulations and Experiments, 11 (2002) 206–217.

[41] S. Rech, A. Surpi, S. Vezzù, A. Patelli, A. Trentin, J. Glor, J. Frodelius, L. Hultman, P. Eklund, Cold-spray deposition of Ti2AlC coatings, Vacuum. 94 (2013) 69–73. https://doi.org/10.1016/J.VACUUM.2013.01.023.

[42] S. Plimpton, Fast Parallel Algorithms for Short – Range Molecular Dynamics, 117 (1995) 1–42.

[43] F. Spaepen, A survey of energies in materials science, Philos. Mag. 85 (2005) 2979–2987. https://doi.org/10.1080/14786430500155080.

[44] A. Stukowski, Structure identification methods for atomistic simulations of crystalline materials, Model. Simul. Mater. Sci. Eng. 20 (2012) 045021. https://doi.org/10.1088/0965-0393/20/4/045021.

[45] A. Stukowski, K. Albe, Extracting dislocations and non-dislocation crystal defects from atomistic simulation data, Model. Simul. Mater. Sci. Eng. 20 (2010) 085001. https://doi.org/10.1088/0965-0393/18/8/085001.

[46] A. Stukowski, V. V Bulatov, A. Arsenlis, Automated identification and indexing of dislocations in crystal interfaces, Model. Simul. Mater. Sci. Eng. 20 (2012) 085007. https://doi.org/10.1088/0965-0393/20/8/085007.

[47] J. Cai, Y.Y. Ye, Simple analytical embedded-atom-potential model including a long-range force for fcc metals and their alloys, Phys. Rev. B. 54 (1996) 8398–8410.

[48] L. Verlet, Computer “Experiments” on Classical Fluids. I. Thermodynamical Properties of Lennard -Jones Molecules, Phys. Rev. 1 (1967) 98–103.

https://doi.org/10.1103/physrev.159.98.

[49] C. Braga, K.P. Travis, A configurational temperature Nosé-Hoover thermostat, J. Chem. Phys. 123 (2005) 134101. https://doi.org/10.1063/1.2013227.

[50] T. Schmidt, F. Gärtner, H. Assadi, H. Kreye, Development of a generalized parameter window for cold spray deposition, Acta Mater. 54 (2006) 729–742. https://doi.org/10.1016/j.actamat.2005.10.005.

[51] C.W. Ziemian, M.M. Sharma, B.D. Bouffard, T. Nissley, T.J. Eden, Effect of substrate surface roughening and cold spray coating on the fatigue life of AA2024 specimens, Mater. Des. 54 (2014) 212–221. https://doi.org/10.1016/j.matdes.2013.08.061.

[52] F. Shimizu, S. Ogata, J. Li, Theory of Shear Banding in Metallic Glasses and Molecular Dynamics Calculations, Mater. Trans. 48 (2007) 2923–2927. https://doi.org/10.2320/matertrans.MJ200769.

[53] S. Rahmati, A. Zúñiga, B. Jodoin, R.G.A. Veiga, Deformation of copper particles upon impact : A molecular dynamics study of cold spray, Comput. Mater. Sci. 171 (2020) 109219. https://doi.org/10.1016/j.commatsci.2019.109219.

[54] K. Wang, J. Liu, Q. Chen, Palladium clusters deposited on the heterogeneous substrates, Appl. Surf. Sci. 376 (2016) 105–112. https://doi.org/10.1016/j.apsusc.2016.02.220.

[55] L.S. Vasil'ev, To the Theory of the Anomalously High Diffusion Rate in Metals under Shock Action : II . Effect of Shear Stresses and Structural and Phase State of the Diffusion Zone on the Rate of Mass Transfer, Phys. Met. Metallogr. 107 (2009) 427–434. https://doi.org/10.1134/S0031918X09050020.

[56] F. Spaepent, A Microscopic Mechanism for Steady State Inhomogeneous Flow in metallic Glass, Acta Mater. 25 (1976) 407–415. https://doi.org/https://doi.org/10.1016/0001-

6160(77)90232-2.

[57] I.E. Gunduz, T. Ando, E. Shattuck, P.Y. Wong, C.C. Doumanidis, Enhanced diffusion and phase transformations during ultrasonic welding of zinc and aluminum, Scr. Mater. 52 (2005) 939–943. https://doi.org/10.1016/j.scriptamat.2004.12.015.

[58] G.D. Zhang, R. Chen, Effect of the interfacial bonding strength on the mechanical properties of metal matrix composites, Compos. Interfaces. 1 (1993) 337–355. https://doi.org/10.1163/156855493x00167.

[59] J. Li, J. Chen, M. Zhu, H. Song, H. Zhang, Interfacial Characteristics of Boron Nitride Nanosheet / Epoxy Resin Nanocomposites : A Molecular Dynamics Simulation, Appl. Sci. 9 (2019) 2832. https://doi.org/10.3390/app9142832.